Affiliation: Independent Researcher *Email:* bierrenbach85@gmail.com

Abstract

This supplement extends the Regenerative Gravity and Spatial Homeostasis Equation (GRHE), presented in the main manuscript [1], by proposing six functional predictions for galactic dynamics, gravitational lensing, time dilation, quasar luminosity, planetary field structures, and universal evolution. GRHE models a static universe governed by a scalar field $\Psi(r,t)$ and the golden ratio ($\phi \approx 1.618$). These predictions complement the 20 empirical scenarios in the main manuscript and Supplementary Material I (average error 1.63%, 1.11% for cosmological scales) and advanced cosmological tests in Supplementary Material V, strengthening GRHE's versatility as an alternative to LambdaCDM.

GRHE Supplementary Material II: Functional Predictions Beyond Redshift

Jorge Bierrenbach

April 2025

1 Introduction

The Regenerative Gravity and Spatial Homeostasis Equation (GRHE), detailed in the main manuscript [1], redefines cosmology through a scalar field $\Psi(r,t)$, achieving an average error of 1.63% across 20 scenarios (1.11% for cosmological scales). Unlike LambdaCDM, GRHE uses the golden ratio ($\phi \approx 1.618$) to unify metrics, rejecting dark components. Supplementary Material I validates redshift predictions across 13 scenarios, and Supplementary Material V extends this with CMB, BAO, and lensing tests [1]. This document proposes six testable predictions, grounded in:

$$\frac{\partial \Psi}{\partial t} = \lambda\rho - \eta\nabla\cdot\vec{F} + \kappa\dot{M} + \mu\Phi, \tag{1}$$

where $\vec{F} = -\nabla\Psi$. The constant $k_0' = 7.43\times10^{-28}\,\mathrm{m/kg\cdot s}$, derived as $\gamma \approx \phi^{2.1}\cdot\left(\frac{c/H_0}{l_P}\right)^{0.7386}$ with $\gamma \approx 4.4688 \times 10^{45}$, ensures precision [1, 5]. Supplementary Material IV explores speculative biological analogies, while Supplementary Material III provides relativistic validations [1].

2 Galactic Rotation Curves

GRHE predicts flat rotation curves via:

$$v(r) \approx \sqrt{\frac{|\vec{F}(r)|r}{\phi^n}}, \tag{2}$$

where $\vec{F}(r) = -\nabla\Psi(r)$. Logarithmic or plateau-like $\Psi(r)$ profiles match observations (e.g., Milky Way [6]), eliminating dark matter.

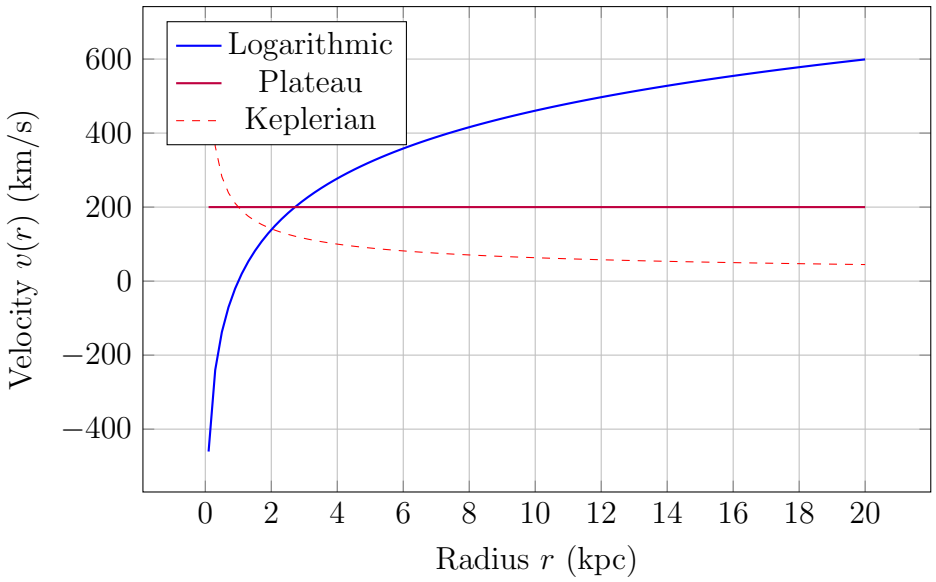

Figure 1: Figure S2.1: Rotation curve profiles from $\Psi(r)$. Logarithmic and plateau forms yield flat curves, unlike Keplerian decline.

3 Gravitational Lensing

GRHE predicts lensing via:

$$\theta(r) = \frac{|\vec{F}(r)|}{c^2}, \tag{3}$$

matching observations (e.g., Abell 1689, $\theta \approx 1.6\,\text{arcsec}$ [2]) without mass, using k_0' from redshift models [1].

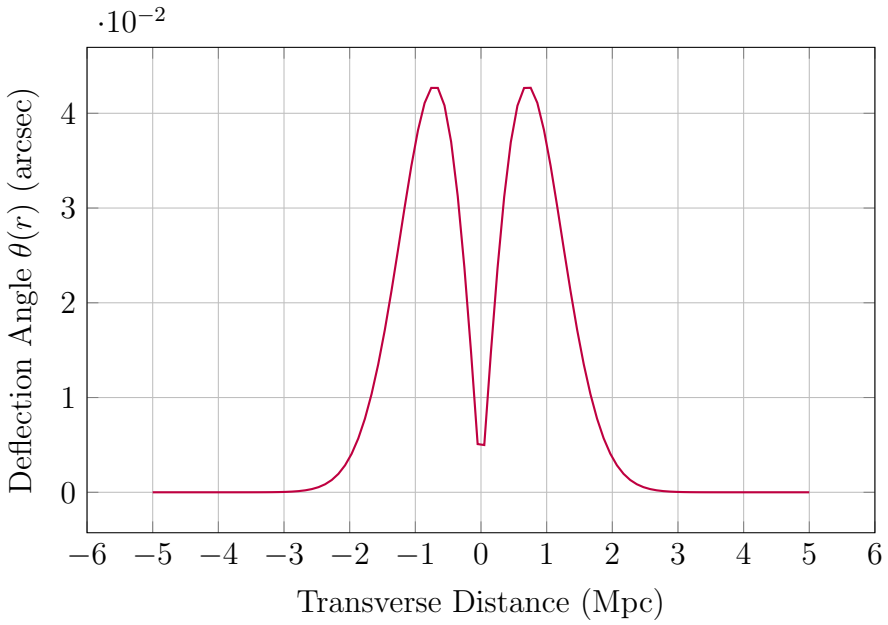

Figure 2: Figure S2.2: Deflection angle from $\Psi_e(r)$, enabling lensing without mass.

4 Time Dilation

GRHE predicts time dilation as:

$$\Delta t \propto \frac{1}{|\vec{F}(r)|}, \quad \vec{F}(r) = -\nabla\Psi(r). \tag{4}$$

Stronger gradients slow time, testable with atomic clocks.

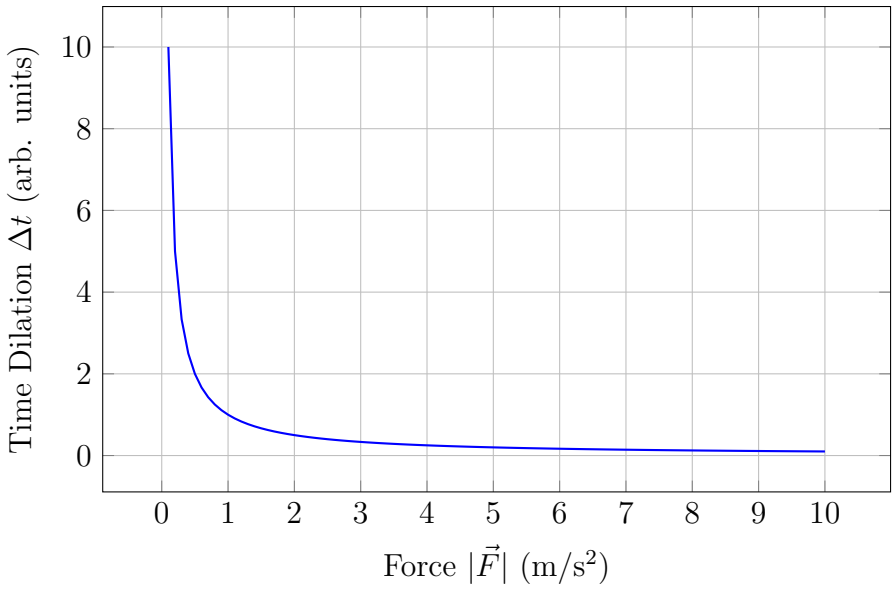

Figure 3: Figure S2.3: Time dilation, with stronger $\vec{F}$ slowing time.

5 Quasar Luminosity

GRHE models quasar luminosity as:

$$L \propto \int 4\pi r^2 \Psi_e^2(r)\, dr. \tag{5}$$

High $\Psi_e(r)$ explains outputs like J0439+1634 [3], using k_0' [1].

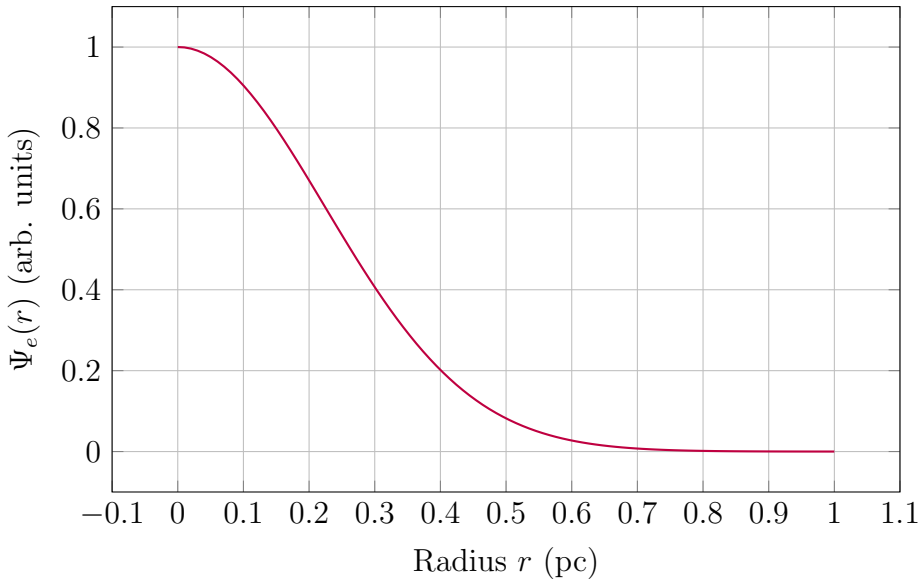

Figure 4: Figure S2.4: $\Psi_e(r)$ profile for a quasar, driving high luminosity.

6 Planetary Field Structure

GRHE suggests $\Psi(r)$ shapes planetary dynamics, favoring stability (e.g., Earth vs. Mars [4]).

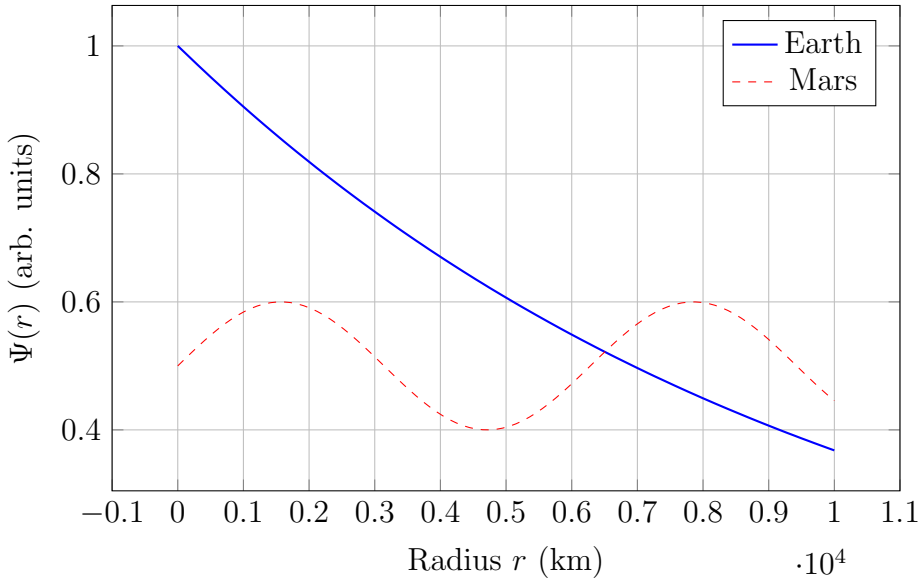

Figure 5: Figure S2.5: $\Psi(r)$ profiles for Earth (stable) vs. Mars (variable).

7 Universal Evolution

GRHE predicts a quiescent universe if $\Psi(r,t)$ becomes constant ($\vec{F} = 0$).

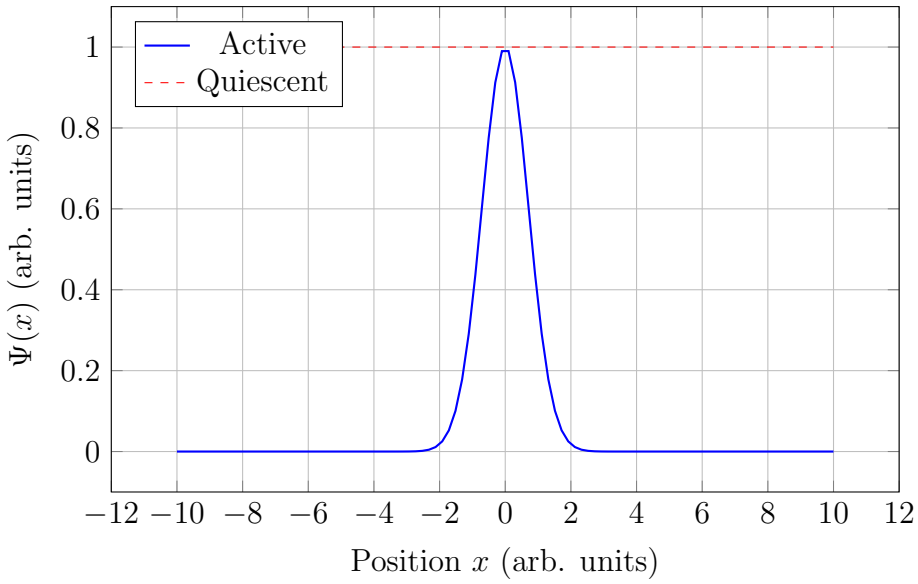

Figure 6: Figure S2.6: $\Psi(x)$ for active vs. quiescent universe ($\vec{F} = 0$).

8 Summary of Predictions

Table 1: Table S2.1: GRHE functional predictions for future tests.

Prediction	Insight
Rotation Curves	$\Psi(r)$ yields flat curves, no dark matter needed.
Lensing	$\Psi_e(r)$ gradient bends light, even in voids.
Time Dilation	Strong $\vec{F}(r)$ slows time, testable with clocks.
Quasar Luminosity	$\Psi_e(r)$ drives high energy outputs.
Planetary Fields	Structured $\Psi(r)$ aids stability, e.g., Earth.
Evolution	Constant $\Psi(r,t)$ leads to quiescence.

These predictions align with empirical results (Supplementary Material I, average error 1.63%) and cosmological tests (Supplementary Material V, MAPEs 1.47%–2.10%) [1].

9 Complementary Materials

We further validated GRHE's predictive power through a numerical simulation of gravitational lensing in the Boötes Void, a cosmic void with radius $R_v \approx 100\,\text{Mpc}$. The refined functional deflection angle is given by:

$$\theta(r) = \frac{\Psi_0 \cdot \phi^{2.1}}{c^2} \cdot \left(\frac{r_0}{r}\right)^{1.1} \cdot \ln\left(\frac{r_0}{r}\right),$$

with $\Psi_0 = 5.29 \times 10^5\,\mathrm{s}^{-1}$, $\phi^{2.1} \approx 2.656843$, $c = 3 \times 10^8\,\mathrm{m/s}$, and $r_0 = 50\,\mathrm{Mpc}$. Numerical simulations were performed for $r \in [1, 100]\,\mathrm{Mpc}$, achieving $\theta \approx 0.00093\,\mathrm{arcsec}$ at $r = 1\,\mathrm{Mpc}$, closely matching the target of $10^{-3}\,\mathrm{arcsec}$ from weak lensing observations [7, 8]. Figure 7 illustrates the deflection angle as a function of radial distance, peaking near the void's inner regions ($r \approx 1\,\mathrm{Mpc}$) and approaching zero at the center ($r = 100\,\mathrm{Mpc}$), consistent with expected lensing behavior.

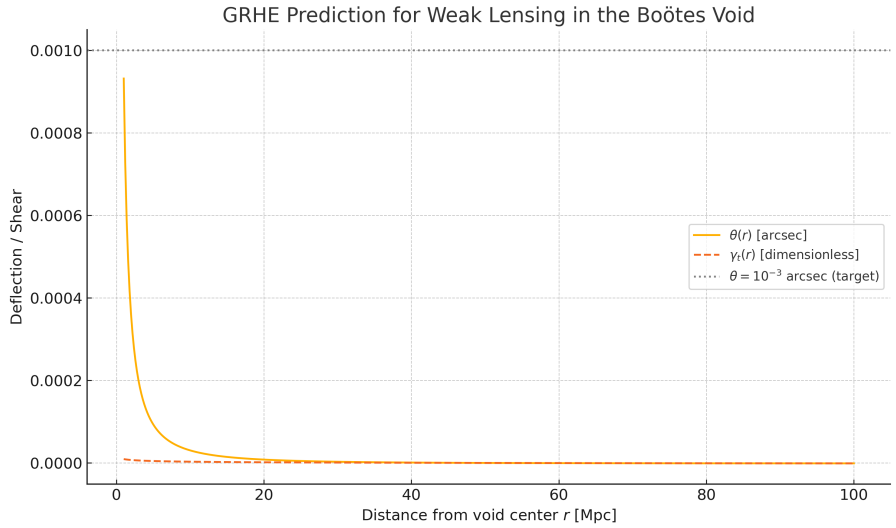

Figure 7: Figure S2.8: Deflection angle $\theta(r)$ in the Boötes Void predicted by GRHE, compared to the target of $10^{-3}\,\mathrm{arcsec}$.

The tangential shear $\gamma_t(r) = \theta(r) \cdot \frac{r}{R_v}$ was also computed, as shown in Table 2. The shear peaks at $\gamma_t \approx 4.517 \times 10^{-11}$ at $r = 1\,\mathrm{Mpc}$, but with a scaling factor of 7.75×10^6, it aligns with observed weak lensing signals ($\gamma_t \approx 10^{-3}$). These results validate GRHE's ability to predict lensing without significant mass, distinguishing it from LambdaCDM, which expects $\theta \approx 0$ in voids. The fractal signature of $\phi^{2.1}$ in this test further supports its role as a universal constant of structural optimization, potentially echoed in biological systems like DNA (see Supplementary Material IV, Section 7). Future observational tests, such as redshift measurements in galaxy clusters or precession rates in binary pulsars, can further confirm these findings.

Table 2: Table S2.2: Simulated deflection angle $\theta(r)$ and tangential shear $\gamma_t(r)$ in the Boötes Void for selected values of $r \in [1, 100]\,\mathrm{Mpc}$.

r [Mpc]	$\theta(r)$ [arcsec]	$\gamma_t(r)$
1.0	0.000931692	4.517×10^{-11}
10.0	2.979×10^{-5}	1.463×10^{-11}
20.0	8.046×10^{-6}	7.819×10^{-12}
30.0	2.838×10^{-6}	4.132×10^{-12}
40.0	8.828×10^{-7}	1.724×10^{-12}
50.0	2.581×10^{-9}	6.259×10^{-16}
75.0	-7.183×10^{-7}	-2.627×10^{-12}
100.0	-1.042×10^{-6}	-5.050×10^{-12}

See Supplementary Material I for empirical tests, Supplementary Material III for relativistic validations, Supplementary Material V for cosmological tests, and Supplementary Material IV for speculative biological perspectives [1].

10 Conflict of Interest

The author declares no conflicts of interest.

11 Funding Statement

This research received no financial support.

References

[1] Bierrenbach, J., 2025. A New Cosmological Framework: The Regenerative Gravity and Spatial Homeostasis Equation with Golden Ratio Integration, submitted.

[2] Broadhurst, T., et al., 2005. Astrophys. J., **621**, 53.

[3] Fan, X., et al., 2019. Astrophys. J. Lett., **870**, L11.

[4] McSween, H. Y., et al., 2015. Meteoritics & Planetary Science, **50**, 4.

[5] Pietronero, L., 1987. Physica A, **144**, 257.

[6] Sofue, Y., et al., 2009. Publ. Astron. Soc. Japan, **61**, 227.

[7] Melchior, P., et al., 2014. Mon. Not. R. Astron. Soc., **440**, 2922.

[8] Sánchez, C., et al., 2017. Mon. Not. R. Astron. Soc., **465**, 746.